Snow Water Equivalent trends in North America through the lens of passive microwave remote sensing and deep learning models

Kristen Kys[1], Isteyak Isteyak[1], Malik Karim[1], Yusriyah Rahman[2], Karanveer Sidhu[2], Hala Al Daker[1]

[1] University of Windsor, School of the Environment, 401 Sunset Avenue, N9B 3P4, Windsor, Ontario, Canada - (kmalik, isteyak, kysk, aldakerh)@uwindsor.ca
[2] University of Windsor, School of Computer Science, 401 Sunset Avenue, N9B 3P4, Windsor, Ontario, Canada - (rahman4n, sidhu66)@uwindsor.ca

Keywords: Snow water equivalent, daily snow trends, siamese U-Net, computer vision, microwave remote sensing.

Abstract

Over the past decades, snow cover trends in North America have been analyzed, providing vital information to the Global Climate Observatory System and other stakeholders about the looming signals of climate-driven snow declines. Detecting daily changes in snow parameters (e.g., depth of snow, extent of snow cover, and snow water equivalent) is, however, fraught with challenges, including internal variability unrelated to climate signals. We used GlobSnow's passive microwave remote sensing data and a convolutional Siamese U-Net to track how snow water equivalent (SWE) changes daily over North America's mid- and high-latitude regions. Daily changes in SWE were detected with F1-scores of 94.8% and 100.0% in locations where it was not trained, and 99.3% at the location where it was primarily trained; this suggests the model's generalization potential to different climatologies and geographic locations. Using the model, we computed a similarity vector to compare SWE trends. We found that although lake-effect snowfall may be prevalent in the Great Lakes Basin during the winter months, the region consistently records the highest frequency of daily changes in SWE. Alaska, Yukon, and the Northwest Territories tended to have minimal daily changes in SWE, suggesting that latitudinal gradients may dominate changes in the snow regime and cryosphere's processes in the warming climate scenarios.

1. Introduction

Snow is classified as an essential climate variable by the Global Climate Observatory System. Snow water equivalent (SWE), depth of snow, and snow cover extent are important parameters that have been widely studied to understand trends in the snow regime and cryosphere processes. SWE is a highly sensitive snow parameter influenced by a variety of climate variables (Thackeray et al., 2019). Upon melting, snow produces water, recharging freshwater systems and contributing to irrigation (Callaghan et al., 2011) and (Bokhorst et al., 2016). Unfortunately, the changing climate is altering the snow regime, resulting in decreasing snow cover and mass across the Northern Hemisphere (Raisanen, 2008). Consequently, a variety of snow data products have been developed to study changes in snow properties. However, the representation of spatial patterns of SWE tends to vary across these datasets. For instance, five snow datasets were studied, revealing consistent snow water mass trends in Winter from $1981-2010$, but with variable strength of SWE representation. GlobSnow SWE and reanalysis data products appeared to consistently represent snow properties in this study (Mudryk et al., 2015).

A profound degree of progress toward detecting and quantifying patterns in SWE variability, depth of snow, snow density, and evaluating snow cover extent has been achieved using gridded SWE datasets. For example, using gridded snow data, SWE trends in Eastern and Western Canada have been shown to decline in March (Brown et al., 2019). Similarly, analysis of the GlobSnows v3.0 dataset showed that snow mass is declining over North America in March (Pulliainen et al., 2020). In many of these studies, however, reference periods and temporal averaging of snow observations are used as the basis for trend analysis. Additionally, March snow data are frequently used to compare trends in SWE. Although these methods have improved our understanding of trends in snow, the use of gridded datasets to study daily snow dynamics at local and regional scales, especially using deep learning methods, remains limited.

Daily changes in SWE have not been extensively studied due to coarse spatial resolution, weak signal-to-noise ratio, snow measurement uncertainties, and natural variability in snow properties that may be unrelated to climate signals. Recently, convolutional siamese networks were applied to detect changes in SWE (Malik and Robertson, 2025), highlighting the potential of deep learning methods to characterize trends in SWE variability. By studying daily changes in the spatial-temporal patterns of snow parameters, we can better predict how snow evolves during the winter months, enabling decision-making regarding the flood risk associated with rapid snow melt and adaptation to potential snow losses due to global warming. The objectives of the study are to: (a) illustrate the potential of passive microwave remote sensing data and deep neural networks to characterize SWE trends over North American mid and high latitudes, and (b) elucidate daily SWE changes in selected climatologies and geographic locations.

2. Study Location

The study area covers the mid and high-latitudes of North America. The Great Lakes Basin (GLB), Quebec, Saskatchewan, Manitoba, and Alberta, which are mid latitudes, and high latitudes – Alaska, Yukon, and the Northwest Territories. These are respectively demarcated as sites A, B, C, D, and E in Figure 1. The majority of the five study sites span multiple provinces; therefore, we give them the following letter designations for simplicity: Alaska,

https://doi.org/10.5194/isprs-archives-XLIX-B3-2026-811-2026

Yukon/Northwest, Manitoba/Saskatchewan/Alberta (MN-SK-AB), and Quebec/Newfoundland-Labrador(QC-NL). In the rest of the sections, we will refer to the five sites using these designations. The data was obtained from GlobSnows v3.0 SWE. GlobSnow v3.0 time series covers the period of 1979 to 2018, and contains daily, monthly, and monthly SWE estimates with bias-correction applied. The spatial resolution of the data is 25 km $\times$ 25 km (Luojus et al., 2021). The dataset masks out Land, Water, and Mountains; thus, negative values are used to denote these features.

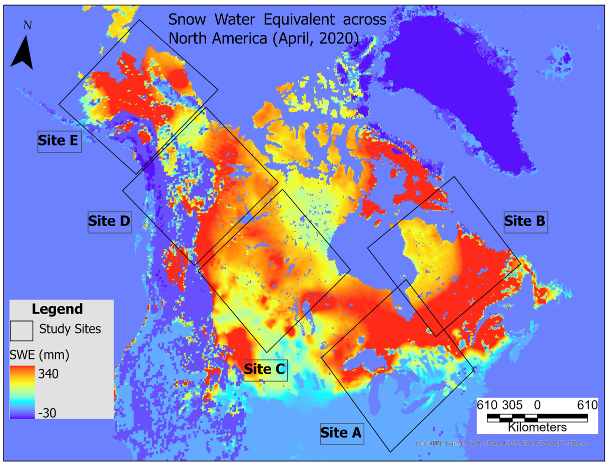

Figure 1. SWE over the Low and Mid latitudes regions in April 2020. Site A(Great Lakes Basin), Site B(QC-NL), Site C(MN-SK-AB,), Site D(Yukon/Northwest), and Site E(Alaska) . Negative values denote land, water, and mountainous areas.

3. Methods for snow property estimation

Satellite-based estimation of snow cover extent, snow density, snow depth, and SWE is commonly accomplished using optical and microwave sensors (Frei et al., 2012). While snow cover estimation may be straightforward for optical sensors, it presents profound limitations associated with cloud cover, vegetation cover, and poor lightning conditions in certain regions. National Oceanic and Atmospheric Administration Interactive Multi-sensor Snow and Ice Mapping System (1998 – 2026) (Chen et al., 2012) and National Aeronautics and Space Administration (NASA) Moderate Resolution Imaging Spectroradiometer (2000 – 2026) (Riggs et al., 2017) snow data are typical optical sensor-derived snow cover products.

Microwave sensors, on the other hand, are capable of estimating snow parameters under all-weather conditions. Their limitation, however, is related to coarse spatial resolution ($>=$ 25 km), as well as uncertainty of snow property estimates in deeper snowpacks (SWE $>$ 150 mm) (Pulliainen et al., 2020). Passive microwave snow datasets include GlobSnow v3.0 and the snow Climate Change Initiative SWE. The GlobSnow v3.0 SWE is generated by combining passive microwave remote sensing through the Multichannel Microwave Radiometer, and Special Sensor Microwave/Imager (SSM/I) and Special Sensor Microwave Imager/Sounder (SSMIS) with ground stations' synoptic measurements of snow depth, application of Bayesian data assimilation techniques, and a Snow Emission model (Luojus et al., 2021).

Global reanalyses are gaining attention, providing estimations of SWE, snowfall, snow mass, and snow cover extent across a variety of climatologies (i.e., mountainous and non-mountain regions). They come in different spatial resolutions and complexity in snow representation. Examples of reanalyses snow products are ERA5-Land from the Copernicus Climate Change Service (Hersbach et al., 2020) and MERRA-2 from NASA (Gelaro et al., 2017). Although these products have improved in terms of snow representation, their relatively low spatial resolution (30 – 60 km) limits the data accuracy (Mortimer et al., 2020).

4. Methodology

4.1 SWE Data Processing

Snow water equivalent data (1979 – 2018) from the GlobSnow website were downloaded, re-projected, and subset to the spatial extents of our study sites – A, B, C, D, and E in Figure 1. We applied normalization using StandardScaler from the Scikit-Learn library, which scales the SWE values to 0 - 1. A fixed spatial extent of 72 $\times$ 72 pixels was adopted as shown in (Malik and Robertson, 2025). This spatial extent enabled the coverage of highly sensitive climatology and regions such as the Great Lakes Basin. We used the geospatial data abstraction library (GDAL) and ArcGIS Pro in tandem to automate the pre-preprocessing phase.

4.2 Model development and training

We adopted the Siamese U-Net model architecture by integrating a computer vision metric – the structural similarity (SSIM) index as a scoring metric into the models last layer (Malik and Robertson, 2025). The SSIM index guides the model to learn the structural differences in SWE using its Encoder-Decoder framework (Figure 2). The contrastive loss function was used for training. We also compared the models performance using the Euclidean Distance metric and binary cross-entropy loss function. The models were trained for 50 epochs, and early stopping with a patience parameter of 5 was used to terminate the training process if a model's performance did not improve after 5 epochs. TensorFlow library, and a computer with an NVIDIA GPU of 20 GB memory was used for model training. SWE data from 1979 – 2001 were used for model training and validation. For independent validation, data from 2002 – 2018 were used. For geographic locations that were not part of the training samples, the independent validation data span 1979 – 2018.

4.3 Training data labeling

We labeled a pair of SWE data as positive (pos) if the dates in which they were sampled differed by 1 day and negative (neg) if the dates of sampling differed by 2 or more days. Using the structural similarity (SSIM) index, we screened the positive and negative labels by setting thresholds. We used the SSIM values greater than or equal to 0.98 for positive SWE (no change instance), and values less than or equal to 0.9 for negative (change instances) (Figure 3). We further augmented this step with human inspection. Samples that were challenging to label as positive or negative pairs were subsequently removed from the training data. The data labeling procedure is extensively described in (Malik and Robertson, 2025).

4.4 Assessment of model accuracy

We computed Precision, Recall – True Positive (TP) rate, False Positive (FP), True Negative (TN), False Negative (FN), and

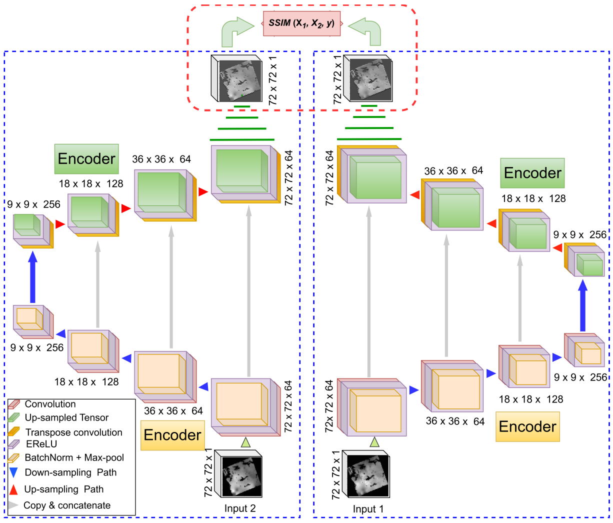

Figure 2. Our Siamese UNet model architecture. The Encoder branches learn to deconstruct SWE, while the Decoder branches reconstruct SWE.

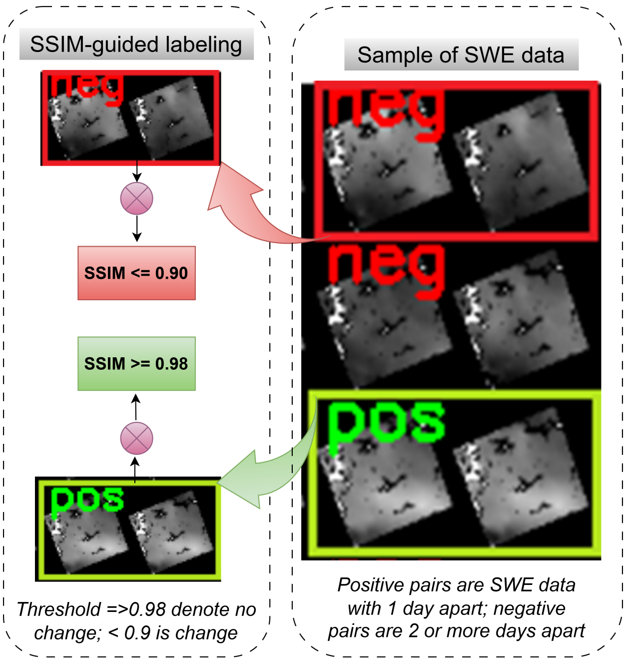

Figure 3. Sample of training data and our labeling workflow

F1-Score to evaluate the models’ capability to detect daily changes in SWE. We further derived the receiver operating characteristics and area under the curve (ROC-AUC) to examine the relationship between true positives and false positives over a range of model thresholds. Equations 1 − 3 denote how the metrics are computed.

$$Precision = \frac{TP}{TP + FP} \tag{1}$$

$$Recall = \frac{TP}{TP + FN} \tag{2}$$

$$F1 - score = \frac{2 \times TP}{2 \times TP + FP + FN} \tag{3}$$

4.5 Computing daily SWE changes

To compute similarity, the Siamese model receives a pair of SWE and outputs a vector of similarity values. High values denote no change; conversely, low values represent a change in SWE. The equation for comparing daily SWE is formulated as shown below, following previous studies (Malik and Robertson, 2025).

$$SWEsim_{(d_i, d_n)} = model\{SWE(d_i, d_{i+1})\}, \tag{4}$$

where d_i represents SWE data sampled on the i^{th} day of the winter months (i.e., JFMA).

5. Results and dicussion

We used a convolutional Siamese UNet to investigate how SWE changes daily over the mid and high-latitude regions of North America. Our modelling framework followed a previous study that deployed a similar deep learning method to characterize SWE trends exclusively in the cold regions of Canada (Malik and Robertson, 2025). Thus, our study extends this work beyond the cold regions and captures daily changes in SWE. Figure 4 presents the ROC-AUC for the model prediction of true and false positives. The ROC-AUC exceeded 90%, suggesting that the model’s predictions are robust. Siamese UNet model’s performance was also evaluated over the different locations, allowing an insight into its potential to generalize to unknown geographic regions and climatology.

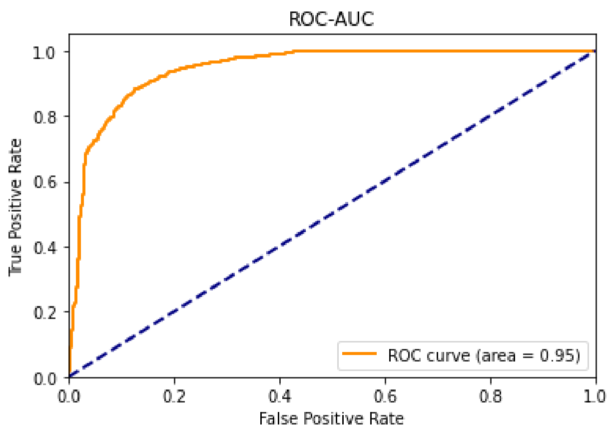

Figure 4. ROC-AUC for U-Net on the independent test data.

Table 1 further sheds light on the model’s prediction accuracy on Sites A, C, and D. Although the model performance was relatively low at Site A (F1-score = 94.84%), it was higher at Sites C and D (99.3% and 100.0%, respectively). It is important to note that the model was trained using data at Site C (from 1979 − 2001), but was tested on SWE data from 2002 − 2018; the test data at Site D ranged from 1979 to 2018, since this location was separate from the training data. Thus, the model’s performance suggests its potential to generalize to different geographic locations and climatology.

Location	Accuracy metric	
	Recall	F1-Score
Site A	99.79	94.84
Site C	98.10	99.30
Site D	100.00	100.00

Table 1. Recall (TPR) and F1-Scores for locations A, C and D.

Figures 5−7 show daily similarities in SWE across the mid and high-latitude regions. We used boxplots to capture the distribution, median, and interquartile ranges (IQR), providing insights into spatial and temporal changes in SWE. We note that high SWE similarity implies less frequent changes; contrarily, low SWE similarity denotes a high degree of change. The similarity trend for SWE tended to remain high between 1989 and 1998 in the high-latitude regions, notably Alaska and Yukon/Northwest (Figure 5). Moreover, the IQRs for the Yukon/Northwest boxplots are short, suggesting that these regions experienced more stable, consistent changes in daily SWE, especially from January to March. Conversely, the IQR for daily changes in April SWE appeared to be more elongated for Yukon/Northwest and QC-NL, indicative of high variability in the April SWE melt-off pattern.

It is also worth noting that QC-NL exhibited high SWE similarity through January to March, though with relatively higher variance, as evidenced in the boxplots' IQR. Thus, these regions may have experienced less severe daily changes in SWE over the decade (i.e., 1989 − 1998). By contrast, the Great Lakes Basin (GLB) and MN-SK-AB experienced profound and competing declines in the underlying daily SWE similarity, suggesting the occurrence of significant daily changes in these regions. For the GLB, the observed SWE decline is a characteristic trend in the eastern and western United States. The snow season is reported to have shortened significantly by 34 days, linked to the later arrival and early ending of the snow season, with temperature and precipitation explaining most of the temporal variation in the patterns of April SWE (Zeng et al., 2018).

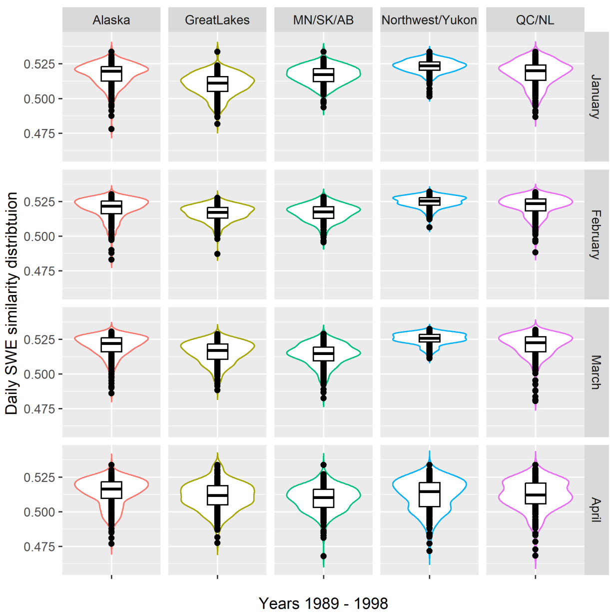

Figure 5. SWE trends from 1979 to 1998.

Figure 6 presents daily SWE from 1999 to 2008. Alaska and Yukon/Northwest dominated the months with high SWE similarity (i.e., less frequent changes in daily SWE), followed by QC-NL. In contrast, profound daily changes characterized the GLB and MN-SK-AB. In January, MN-SK-AB exhibited relatively higher SWE similarity than the GLB, yet a pattern of declining similarity, corresponding to increased daily changes, persisted across the other winter months (i.e., February, March, and April). Although snow cover is reported to have declined in the northeastern United States and eastern Canada (Contosta et al., 2019), our findings point to regional and climatological variation in SWE trends − high and low rates of change in the mid and high latitudes, respectively. Surprisingly, toward the end of the winter (i.e., April), the four regions tended to exhibit a similar distribution, except for QC-NL, where the IQR points to more dispersion, indicating that a highly varying daily SWE melt-off pattern tended to dominate the region at the end of winter.

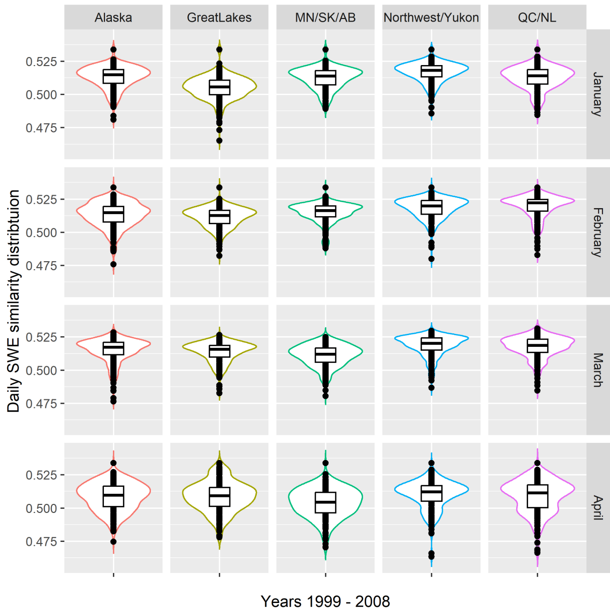

Figure 6. SWE trends from 1999 to 2008.

Figure 7 SWE shows a relatively lower similarity (profound change) in the GLB in January, whereas the other regions depict high similarity but are regionally variable. Late arrival of snow in southern Ontario and the northern parts of the Conterminous United States likely drives the low SWE in GLB (Zeng et al., 2018). Yukon and the Northwest Territories tend to have the highest SWE similarity; however, the trend tended to be similar to Alaska. The pattern of SWE distribution in February across the 5 locations follows the trend observed in January; yet, there is less variability in the similarity values (as shown by the violin and box plots). This suggests consistent snow accumulation and less melt, leading to many areas being similar. Despite the relatively high variability, QC-NL exhibited high SWE similarity with the Yukon/Northwest and Alaska in March. The relatively high SWE similarity for QC-NL in March appears to be a surprising trend, given that it is at mid latitudes compared to Yukon/Northwest and Alaska.

In April, SWE similarity tended to be the lowest for MN-SK-AB than for the other 4 regions. The GLB surprisingly showed higher SWE similarity than MN-SK-AB. However, a careful assessment of the data revealed that the Winter season might have ended early in April, causing most of the areas to have no snow and thus, appear similar. MN-SK-AB, on the other hand, had pockets of snow on the ground, whose variable melt-off pattern is detected by the model, leading to low similarity. This points to the complexity of snow dynamics and cryosphere processes that may be unfolding in specific regions (Pederson et al., 2013).

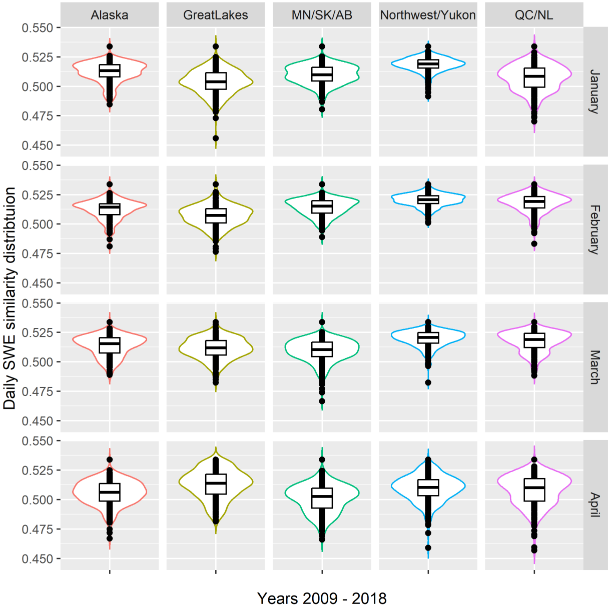

Figure 7. SWE trends from 2009 to 2018.

6. Conclusion

We assessed the capabilities of a convolutional Siamese U-Net to detect changes in daily SWE across selected regions in North America. By incorporating the SSIM index into the U-Net architecture, its detection capability improved, achieving a 99.3% F1-score in characterizing scenarios of change and no change in SWE. Using the model, we derived time-series vectors to characterize multi-decadal SWE trends (i.e., from 1989 – 2018) over the mid and high latitude regions of North America. SWE similarity tended to be higher in Alaska, Yukon, and the Northwest Territories throughout JFMA than in the other regions. Quebec and Newfoundland-Labrador also exhibited higher SWE similarity in March than Saskatchewan, Alberta, and Manitoba. Despite the potential occurrence of lake-effect snowfall, the GLB appears to be the region with consistently low SWE similarity throughout the winter season, a characteristic that reflects the pattern of declining snowpack levels in the northeastern United States and eastern Canada.

We note that different datasets exhibit variable stability and consistencies in SWE representation – climatology and meteorology (Urraca and Gobron, 2023). For example, it was found that spatial patterns of SWE in existing gridded datasets are not entirely consistent over different regions (e.g., boreal forest, Arctic, and Alpine regions) (Mudryk et al., 2015). Consequently, future work that focuses on analyzing diverse SWE datasets and linking observed trends to climate variables (e.g., temperature and precipitation) holds the potential to improve our understanding of daily changes in SWE. Lastly, diverse deep models may capture SWE patterns with different magnitudes of change and similarity; thus, it would be worth exploring the capability of other learning model architectures (e.g., Vision Transformers and Residual Networks) and computer vision metrics such as the multiscale SSIM and the complex wavelet structure similarity index to characterize trends in SWE. The next phase of our research will tackle these two pivotal points.

Acknowledgment

The authors acknowledge the University of Windsor's support in conducting this research by providing the necessary resources (GPU-enabled computers, ArcGIS Pro licenses, etc)

References

Bokhorst, S., Pedersen, S. H., Brucker, L., Anisimov, O., Bjerke, J. W., Brown, R. D., Ehrich, D., Essery, R. L., Heilig, A., Ingvander, S., Johansson, C., Johansson, M., Jnsdttir, I. S., Inga, N., Luojus, K., Macelloni, G., Mariash, H., McLennan, D., Rosqvist, G. N., Sato, A., Savela, H., Schneebeli, M., Sokolov, A., Sokratov, S. A., Terzago, S., Vikhamar-Schuler, D., Williamson, S., Qiu, Y., Callaghan, T. V., 2016. Changing arctic snow cover: A review of recent developments and assessment of future needs for observations, modelling, and impacts.

Brown, R. D., Fang, B., Mudryk, L., 2019. Update of Canadian Historical Snow Survey Data and Analysis of Snow Water Equivalent Trends, 19672016. *Atmosphere - Ocean*, 57, 149-156. https://doi.org/10.1080/07055900.2019.1598843.

Callaghan, T. V., Johansson, M., Brown, R. D., Groisman, P. Y., Labba, N., Radionov, V., Bradley, R. S., Blangy, S., Bulygina, O. N., Christensen, T. R., Colman, J. E., Essery, R. L., Forbes, B. C., Forchhammer, M. C., Golubev, V. N., Honrath, R. E., Juday, G. P., Meshcherskaya, A. V., Phoenix, G. K., Pomeroy, J., Rautio, A., Robinson, D. A., Schmidt, N. M., Serreze, M. C., Shevchenko, V. P., Shiklomanov, A. I., Shmakin, A. B., Skold, P., Sturm, M., Woo, M. K., Wood, E. F., 2011. Multiple effects of changes in arctic snow cover. *Ambio*, 40, 32-45.

Chen, C., Lakhankar, T., Romanov, P., Helfrich, S., Powell, A., Khanbilvardi, R., 2012. Validation of NOAA-interactive multisensor snow and Ice Mapping System (IMS) by comparison with ground-based measurements over continental United States. *Remote Sensing*, 4, 1134-1145.

Contosta, A. R., Casson, N. J., Garlick, S., Nelson, S. J., Ayres, M. P., Burakowski, E. A., Campbell, J., Creed, I., Eimers, C., Evans, C., Fernandez, I., Fuss, C., Huntington, T., Patel, K., Sanders-DeMott, R., Son, K., Templer, P., Thornbrugh, C., 2019. Northern forest winters have lost cold, snowy conditions that are important for ecosystems and human communities. *Ecological Applications*, 29.

Frei, A., Tedesco, M., Lee, S., Foster, J., Hall, D. K., Kelly, R., Robinson, D. A., 2012. A review of global satellite-derived snow products. *Advances in Space Research*, 50, 1007-1029.

Gelaro, R., McCarty, W., Surez, M. J., Todling, R., Molod, A., Takacs, L., Randles, C. A., Darmenov, A., Bosilovich, M. G., Reichle, R., Wargan, K., Coy, L., Cullather, R., Draper, C., Akella, S., Buchard, V., Conaty, A., da Silva, A. M., Gu, W., Kim, G. K., Koster, R., Lucchesi, R., Merkova, D., Nielsen, J. E., Partyka, G., Pawson, S., Putman, W., Rienecker, M., Schubert, S. D., Sienkiewicz, M., Zhao, B., 2017. The modern-era retrospective analysis for research and applications, version 2 (MERRA-2). *Journal of Climate*, 30, 5419-5454.

Hersbach, H., Bell, B., Berrisford, P., Hirahara, S., Hornyi, A., Muoz-Sabater, J., Nicolas, J., Peubey, C., Radu, R., Schepers, D., Simmons, A., Soci, C., Abdalla, S., Abellan, X., Balsamo, G., Bechtold, P., Biavati, G., Bidlot, J., Bonavita, M., Chiara, G. D., Dahlgren, P., Dee, D., Diamantakis, M., Dragani, R., Flemming, J., Forbes, R., Fuentes, M., Geer, A., Haimberger, L., Healy, S., Hogan, R. J., Hlm, E., Janiskov, M., Keeley, S., Laloyaux, P., Lopez, P., Lupu, C., Radnoti, G., de Rosnay, P., Rozum, I., Vamborg, F., Villaume, S., Thpaut, J. N., 2020. The ERA5 global reanalysis. *Quarterly Journal of the Royal Meteorological Society*, 146, 1999-2049.

Luojus, K., Pulliainen, J., Takala, M., Lemmetyinen, J., Mortimer, C., Derksen, C., Mudryk, L., Moisander, M., Hiltunen, M., Smolander, T., Ikonen, J., Cohen, J., Salminen, M., Norberg, J., Veijola, K., Venlinen, P., 2021. GlobSnow v3.0 Northern Hemisphere snow water equivalent dataset. *Scientific Data*, 8, 1-16.

Malik, K., Robertson, C., 2025. Structural Similarity-Guided Siamese U-Net Model for Detecting Changes in Snow Water Equivalent. *Remote Sensing*, 17, 1631. https://www.mdpi.com/2072-4292/17/9/1631.

Mortimer, C., Mudryk, L., Derksen, C., Luojus, K., Brown, R., Kelly, R., Tedesco, M., 2020. Evaluation of long-term Northern Hemisphere snow water equivalent products. *Cryosphere*, 14, 1579-1594.

Mudryk, L. R., Derksen, C., Kushner, P. J., Brown, R., 2015. Characterization of Northern Hemisphere snow water equivalent datasets, 1981-2010. *Journal of Climate*, 28, 8037-8051.

Pederson, G. T., Betancourt, J. L., McCabe, G. J., 2013. Regional patterns and proximal causes of the recent snowpack decline in the Rocky Mountains, U.S. *Geophysical Research Letters*, 40, 1811-1816.

Pulliainen, J., Luojus, K., Derksen, C., Mudryk, L., Lemmetyinen, J., Salminen, M., Ikonen, J., Takala, M., Cohen, J., Smolander, T., Norberg, J., 2020. Patterns and trends of Northern Hemisphere snow mass from 1980 to 2018. *Nature*, 581, 294-298. http://dx.doi.org/10.1038/s41586-020-2258-0.

Raisanen, J., 2008. Warmer climate: Less or more snow? *Climate Dynamics*, 30, 307-319.

Riggs, G. A., Hall, D. K., Romn, M. O., 2017. Overview of NASA’s MODIS and Visible Infrared Imaging Radiometer Suite (VIIRS) snow-cover Earth System Data Records. *Earth System Science Data*, 9, 765-777.

Thackeray, C. W., Derksen, C., Fletcher, C. G., Hall, A., 2019. Snow and climate: Feedbacks, drivers, and indices of change.

Urraca, R., Gobron, N., 2023. Temporal stability of long-term satellite and reanalysis products to monitor snow cover trends. *Cryosphere*, 17, 1023-1052.

Zeng, X., Broxton, P., Dawson, N., 2018. Snowpack Change From 1982 to 2016 Over Conterminous United States. *Geophysical Research Letters*, 45, 12,940-12,947.